

A comparative Fluid-Structure Interaction study of stenosed and normal Common Carotid Artery

S. M. Abdul Khader^{1*}, B. S. Shenoy¹, B. Raghuvir Pai¹, N. S. Mahmood², G. Kamath³, V. R. K Rao²

¹ Department of Mechanical Engineering, Manipal Institute of Technology, Manipal University, Manipal 576104, India

² Department of Radio-Diagnosis and Imaging, Kasturba Medical College, Manipal University, Manipal 576104, India

³ Department of Cardio-Thoracic Surgery, Kasturba Hospital, Manipal University, Manipal 576104, India

(Received August 22 2008, Accepted June 25 2009)

Abstract. Fluid-Structure Interaction (FSI) is one of the growing challenges in recent times, wherein both fluid and structural solution domains are coupled using CFD and FEM methods respectively. Results from both the analysis are exchanged at interface junction in a synchronized manner to obtain an FSI solution. This study is helpful in observing the behavior of blood flow through arteries and to study the mechanisms of diseases like Atherosclerosis, Hypertension, Aneurysms etc. The blood flow distends the elastic artery due the flow-induced pressure and deformed artery in turn affects the flow behavior. The prime concern is in this study is to compare the change in flow behavior and structural displacement of both occluded and normal carotid artery. The clinical data is obtained from ultrasound technique and the subject is having an eccentric occlusion of 66% in left common carotid and right common carotid shows normal behavior. Initially, the CFD model is analyzed considering the realistic physiological boundary conditions. Then FSI model is analyzed considering the same boundary conditions as observed for that of CFD model. The modeling and analysis is carried out using ANSYS, commercially available Finite Element software. An ANSYS Parametric Design Language (APDL) has been written to carry out the transient analysis and the parameters like arterial deformation, flow velocity and wall shear stress are considered. The results obtained agree well with the clinical observations and theoretical values.

Keywords: FSI, stenosed carotid artery, ANSYS APDL, CFD of arterial flow

1 Introduction

Blood flow characteristics in arteries can be altered significantly by arterial disease, such as stenosis and aneurysms. The altered haemodynamics may further influence the development of the disease and arterial deformity and change the regional blood rheology. The study of physiologically realistic pulsatile flow through stenosis has profound implications for the diagnosis and treatment of vascular disease.

Although the actual geometry of a stenosis artery may be varied and complex, it has been frequently simplified as symmetrical or asymmetrical constriction in a cylindrical tube. In general, flow through constricted tubes is characterized by a high velocity jet generated from the narrowest section and flow separation distal to the stenosis. Even though the pre-stenotic flow is usually laminar, flow in the post-stenotic region could become highly disordered or even turbulent depending upon the flow conditions and severity of the stenosis. Understanding of stenotic flow has also proceeded from both theoretical and computational efforts.

The post-stenotic phenomenon has been studied by Long et al.^[7] on a straight tube stenosed model. In this study axisymmetrical and symmetrical model with a reduction of 25%, 50% and 75% were constructed. The results have demonstrated that the formulation and development of FSZ in poststenotic region are complex in flow deceleration zone. While Bathe and Kamm^[1] used the “iterative over time step” coupling approach in

* Corresponding author. E-mail address: smak.quadri@gmail.com.

modeling pulsatile flow in stenotic arteries. Boundary conditions at the inlet and outlet were obtained from experimental data. Their model was compared with other mathematical models and was validated against experimental data. They compared arteries with different degrees of stenoses. The iterative approach for flow field has been examined by Perktold and Rappitsch^[10]. The boundary conditions of the flow problem, the inlet and the outlet pressure, were obtained from experimental data.

The similar study on stenotic arteries has been carried out by Tang et al.^[14] by using both thick and thin wall model. They noticed that the stenotic severity and asymmetry in thick wall models changed not only the wall geometry, but also the stiffness of the tube wall and this affected the wall deformation. They came to the conclusion that arteries have a complex structure and should not be treated as a homogenous material. Later Tang et al.^[13] introduced a nonlinear three-dimensional thick-wall model with fluid-structure interactions to simulate blood flow in carotid arteries with an asymmetric stenosis to quantify the effects of stenosis severity, eccentricity, and pressure conditions on blood flow and artery compression.

In the present study the change in flow and structural behavior is compared on a realistic CCA model considering both the normal as well as occluded artery. The radial displacements, Wall Shear Stress and Flow Separation Zone are compared in both normal and occluded cases.

2 Methods and model description

2.1 Governing equations of FSI solution

Contributions to WJMS are welcome from throughout the world. Manuscripts may be submitted to the managing editor In FSI analysis, the fluid domain is solved using modified momentum equation adopting moving velocity is used along with continuity equation as given in equation below^[2].

$$\frac{\partial}{\partial t} \int_{\Omega} \rho \partial \Omega + \int_S \rho (v - v_b) \cdot n \partial S = \int_S (\tau_{ij} i_j - P i_i) \cdot n \cdot \partial S + \int_{\Omega} b_i \partial \Omega,$$

where ρ is the density, τ is the stress tensor, v is the velocity vector, v_b is the grid velocity, P is the pressure, b_i is the body force at time t .

The transient dynamic structural solution is given by equation below^[5]. The stiffness matrix is updated in each time step. The Newmark method is used for updating of displacement at each time interval and then stiffness matrix is solved using direct solver in particular sparse solver, for every time step.

$$[M]\{\ddot{U}\} + [C]\{\dot{U}\} + [K]\{U\} = \{F^a\}.$$

Where M is the structural mass matrix, C is the structural damping matrix, K is structural stiffness matrix, F^a is the applied load vector and \ddot{U} , \dot{U} and U represents acceleration, velocity and displacement vector.

2.2 FSI algorithm

The FSI analysis is performed using sequentially coupled FSI solver in ANSYS^[5, 6]. This solver uses ANSYS FLOTRAN elements for fluid domain and ANSYS structural for solid domain. The FSI algorithm is shown in form of flow chart in Fig. 1. In the beginning of the FSI analysis, first fluid domain has to be modeled using appropriate element then required boundary conditions are applied followed by solid domain. The FSI algorithm solves the fluid and solid domains independently. After fluid domain is solved, the surface load to the solid domain is transferred through fluid-structure interface and solid domain gets solved. After the convergence is achieved, the fluid mesh has to be morphed using Arbitrary Lagrangian-Eulerian (ALE) formulation. The algorithm continues to loop through the solid and fluid domain until convergence is reached for that time step. Later the loop continues to solve for the time period specified.

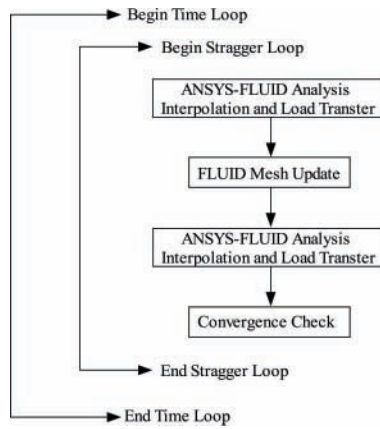


Fig. 1. FSI algorithm

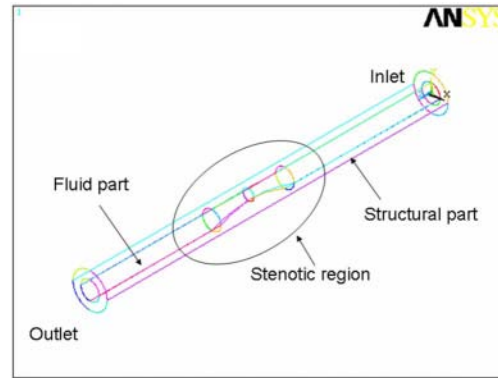


Fig. 2. Occluded model for left CCA

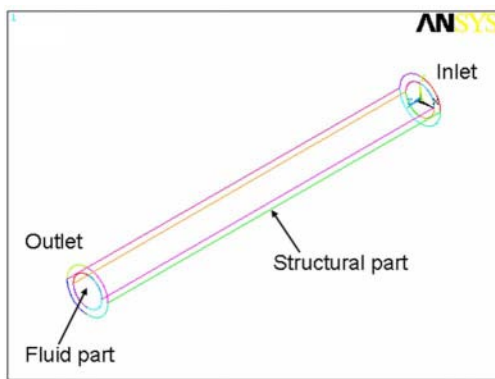


Fig. 3. Normal model for right CCA

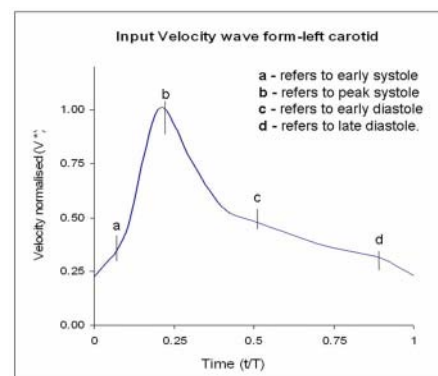


Fig. 4. Inlet Velocity wave form

2.3 FSI model description

An approximate carotid model of both the sides is generated in ANSYS-10.0. The required details are obtained from Duplex scan done on an old patient, who is having 66% eccentric occlusion in left side and right side is observed to be normal as shown in Fig. 2 and Fig. 3 respectively. The details of both the sides are taken at different sections depending upon the convenience using M-mode scan for velocity and B-mode scan for diastolic diameter^[10, 15]. The geometry of models in this study is generated having a length of 15D and thickness of solid model is 0.15D.

3 Analysis

Both fluid and structural part are modeled with 8 noded brick element and discretized into hexahedral elements with fluid part comprising of approximately 50000 element and structural part having 12000^[10, 15]. In this case, one pulse cycle is discretized into 50 time steps to simulate the flow behavior more accurately. The normalized inlet velocity waveform is shown in Fig. 4 and constant pressure boundary conditions at outlet for fluid-model^[13, 14]. The inlet velocity profile shown in Fig. 4 is for occluded left CCA, where the distal flow is more than compared to that of normal right CCA. The inlet and outlet of solid model is constrained in all directions^[15]. The density of the fluid domain is 1050 kg/m^3 and dynamic viscosity is 0.004 N-sec/m^2 , while density of solid domain is 1120 kg/m^3 , Poisson's ratio is 0.40 and elastic modulus is 0.9Mpa. Since the patient is aged person, the arterial wall is stiffened and elasticity is less when compared with that of healthy young persons. Due to this stiffening, there is a change in Elastic modulus and Poisson's ratio as seen from Raymond G et al.^[11], W. A. Riley et al.^[12], Mc Donald^[9], Jay Humprey^[4] and Fung^[3]. A generalized APDL written in ANSYS performs the creation of geometry, solution and post processing of results.

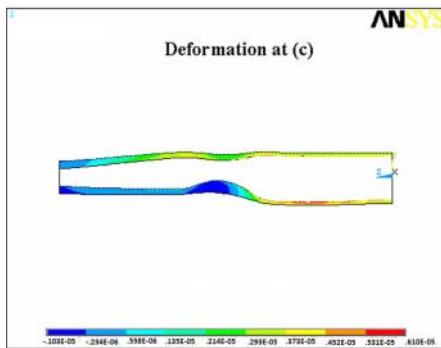


Fig. 5. Occluded model for left CCA

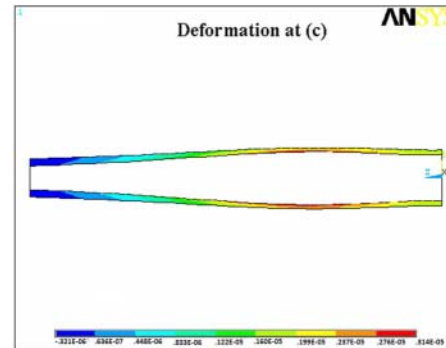


Fig. 6. Normal model for right CCA

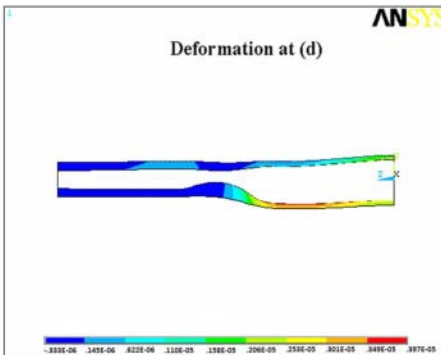


Fig. 7. Occluded model for left CCA

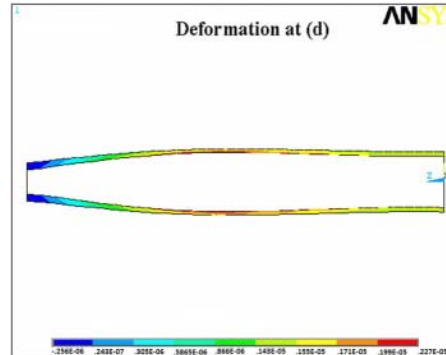


Fig. 8. Normal model for right CCA

4 Results and discussions

The computed results like numerical values of displacement, wall shear stress and velocity patterns are normalized to facilitate the comparison purpose. The structural displacement patterns are shown in Fig. 5 to Fig. 8, which are obtained at selected instants of pulse cycle as shown in Fig. 4 and maximum displacement is observed at systolic phase i.e. at instant (b). The flow and displacement pattern are normal as observed clinically in healthy people. The radial distention seen in Fig. 6 and Fig. 8 is for normal right CCA at instant (c) and (d) of pulse cycle, which is compared with occluded left CCA for similar instants as seen in Fig. 5 and Fig. 7. The post-stenotic distention seen in Fig. 5 is prime focus for occlusions and obtained results are comparable as observed clinically. The flow increases in vicinity of occlusion which leads to jet formation in downstream causing post-stenotic distention and though this distention subsides at instant (d), but eddies are formed causing turbulence in downstream side and pressure accumulation in upstream side.

The radial distention is compared with theoretical calculations^[8] for both normal and occluded models as seen in Fig. 9 and Fig. 10. In case of normal model, the comparison is more similar, though during diastolic flow, there is some difference, which is due to flow deceleration as observed clinically. Also in early part of cycle, the difference is because the artery has lost its elasticity and flow requires time to propagate smoothly. Then in case of occluded model, large difference is observed as flow accumulates in upstream prior to occlusion and increases the pressure and another reason may be due to numerical approximation.

Because of these reasons even in case of Wall shear stress plots, shown in Fig. 11 and Fig. 12 for occluded and normal model respectively. The initial difference is observed at instants (a) and (b) for normal model (Fig. 12) and smooth variation is absent for rest of the pulse cycle. Due to the structural flexibility, the WSS is more in case of rigid model (CFD model) than flexible model (FSI) as fluid undergoes more shearing in CFD model than in FSI model as elastic structure dampens the flow induced pressure. Also in the flexible WSS plot during the late diastole period there is slight increase in the WSS, this is mainly due to the diastolic flow, which increases the shearing effect due to back flow^[10, 14, 15]. In case of occluded model, the comparison is not the same as that observed in normal model. The rigid WSS plot increases exponentially whereas the flexible WSS plot follows the sharp rise and decline during systolic and diastolic flow respectively. This is because in

rigid WSS plot, the shearing of fluid continues even during the later part of pulse cycle, where as in case of flexible WSS plot, the structure dampens the flow induced pressure.

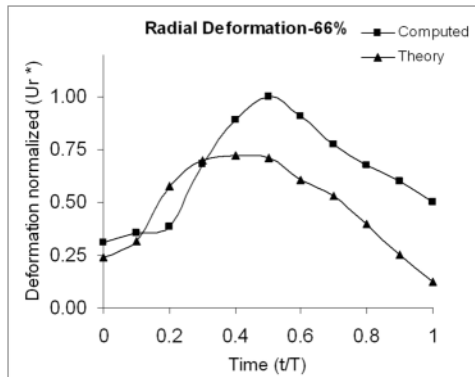


Fig. 9. Occluded model for left CCA

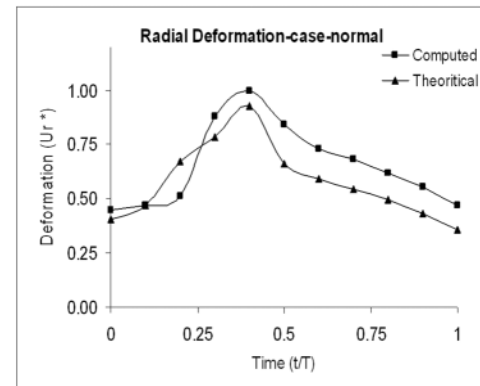


Fig. 10. Normal model for right CCA

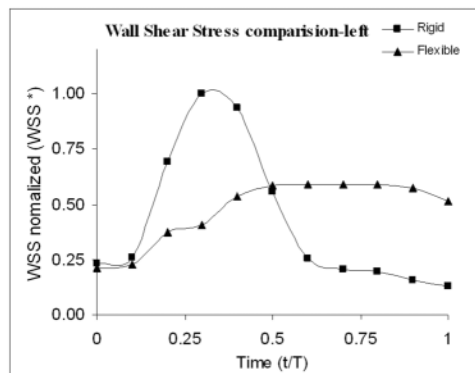


Fig. 11. Occluded model for left CCA

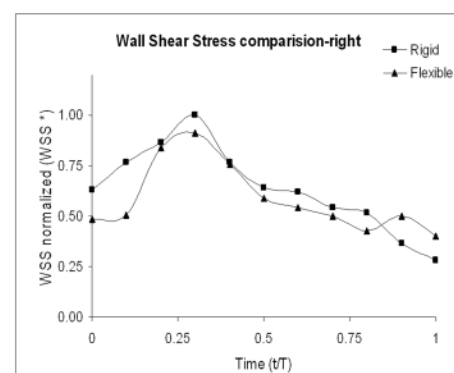


Fig. 12. Normal model for right CCA

5 Conclusion

(1) In present case study, the person is having 66% occlusion in left sided common carotid artery and right sided one is normal. For both the cases, CFD and FSI analysis is carried out.

(2) The diastolic flow is more in occluded model than in normal model due to occlusion.

(3) Due to old age, the artery has stiffened and the change in structural property is included in the model.

(4) The post-stenotic distention is observed in downstream of occluded model similar to that clinically observed behavior, while the right CCA shows the normal distention.

(5) The computed and theoretical radial displacement comparison of right CCA is observed to be normal and difference is due to flow deceleration and numerical approximation. But for occluded model, large difference is observed due to pressure accumulation prior to occlusion.

(6) The rigid and flexible WSS plots are compared separately for occluded and normal model. In normal model, the rigid domain shows more WSS than flexible model as given in available literature. But there is sharp rise and decline during systolic flow in case of occluded model comparison.

(7) The flow separates in downstream and eddies are formed causing turbulence.

References

- [1] M. Bathe, R. Kamm. A fluidstructure interaction finite element analysis of pulsatile blood flow through a compliant stenotic artery. *Journal of Biomechanical Engineering Transactions of the ASME*, 1999, **121**: 361–369.

- [2] J. Ferziger, M. Peric. Computational Methods for Fluid Dynamics. Berlin Heidelberg, 2002.
- [3] Y. Fung. *Biodynamics-Circulation*. Springer Verlag, 1984. New York Inc.
- [4] J. Humphrey, S. Delange. *An Introduction to Biomechanics*. Springer Verlag, 2004. New York Inc.
- [5] A. Inc. *ANSYS Release 9.0 Documentation*. ANSYS Company, Pittsburgh, 2003. PA.
- [6] Z. Li, C. Kleinstreuer. FluidStructure Interaction Effects on SacBlood Pressure and Wall Stress in a Stented Aneurysm. *Transactions of the ASME*, 2005, **127**: 662–671.
- [7] Q. Long, X. Xu, et al. Numerical investigations of physiological pulsatile flow through arterial stenosis. *Journal of Biomechanics*, 2001, **34**: 1229–1242.
- [8] S. Middleman. *Transport Phenomena in the Cardiovascular System*. WileyInterscience Inc., 1972.
- [9] W. Nichols, M. O'Rourke. *McDonald's Blood Flow in Arteries*. LEA & FEBIGER, Philadelphia, London, 1998.
- [10] K. Perktold, G. Rappitsch. Computer simulation of local blood flow and vessel mechanics in a compliant carotid artery bifurcation model. *Journal of Biomechanics*, 1995, **25**: 845–856.
- [11] G. Raymond, M. Budge. Terminology for Describing Elastic behavior of Arteries. *Hypertension*, 2003, **41**: 1180–1182.
- [12] W. Riley, R. Barnes, et al. Ultrasonic measurement of the elastic modulus of the common carotid. *Stroke*, 1992, **23**: 952–956. The Atherosclerosis Risk in Communities (ARIC) Study.
- [13] D. Tang, S. Kobayashi, J. Zheng. Effect of Stenosis Asymmetry on Blood Flow and Artery Compression: A Three-Dimensional FluidStructure Interaction Model. *Annals of Biomedical Engineering*, 2003, **31**(10): 1182–1193.
- [14] D. Tang, C. Yang, et al. Wall stress and strain analysis using a 3D thick-wall model with fluid-structure interactions for blood flow in carotid arteries with stenoses. *Computers and Structures*, 1999, **72**: 341–356.
- [15] S. Zhao, X. Xu, M. Collins. Blood flow and vessel mechanics in physiological realistic model of a human carotid arterial bifurcation. *Journal of Biomechanics*, 2000, **32**: 975–984.

Appendix

| | | | |
|--------------------|---|------------------|--|
| CCA | : Common Carotid Artery | D^* | : Normalized diameter = D_t/D_{\max} |
| D_t | : Diameter at time, t | D_{\max} | : Maximum diameter in time period |
| U_r^* | : Normalized radial displacement = U_t/U_{\max} | U_t | : Radial displacement at time, t |
| U_{\max} | : Maximum radial displacement in time period | U_r | : Radial displacement at radius, r |
| V^* | : Normalized velocity = V_t/V_{\max} | V_t | : Velocity at time, t |
| V_{\max} | : Maximum velocity in time period | WSS _t | : WSS at time, t |
| WSS* | : Normalized Wall Shear Stress = WSS_t/WSS_{\max} | S | : Closed surface |
| WSS _{max} | : Maximum WSS in time period | Ω | : Control volume |

Fig. 11 shows variation of the pressure (mid-plane) developed in the circumferential direction for bearing with $L/D = 1.0$ for different values of ε . Similarly, Fig. 12 illustrates the effect of various L/D on the pressure distribution for $\varepsilon = 0.6$. From Fig. 11 and Fig. 12 it is clear that ε has greater influence on the pressure than L/D ratios. Fig. 13 compares the maximum deformation of the bearing structure with various L/D and ε . From Fig. 13 it is observed that an increase in ε predominantly increases δ_{\max} .

6 Conclusions

The overall EHL analysis of full journal bearing (360°) has been conducted using the sequential application of Computational Fluid Dynamics (CFD) and Computational Structural Dynamics (CSD). General FSI codes makes the analysis effective where complex flow geometries are involved or when more detailed solutions are needed. The simulation results of Elasto-hydrodynamic lubrication have a good agreement with that of the standard lubrication solutions. These techniques has been successfully implemented in finding the bearing surface deformation under static load and the approach can be extended in predicting the bearing performance under dynamic loading condition. Eventually FSI analysis will play a very important role in the field of fluid film bearing analysis.

References

- [1] P. Allaire, J. Nicholas, E. Gunter. Systems of Finite Elements for finite bearings. *ASME Journal of Lubrication Technology*, 1972, (99): 187–197.
- [2] P. Bhat, B. Shenoy, R. Pai. Elasto-hydrodynamic Lubrication Analysis of a Radially Adjustable Partial Arc Bearing Using Fluid Structure Interaction. **in:** *Proc. of ASME/STLE International Joint Tribology Conference*, San Diego, California, US, 2007, 1–3. IJTC'07, IJTC44479.
- [3] J. Booker, K. Huebner. Application of Finite Element Methods to Lubrication: an Engineering Approach. *ASME Journal of Lubrication Technology*, 1972, (94): 313–323.
- [4] P. Brajdic-Mitidieri, A. Gosman, et al. CFD Analysis of a Low Friction Pocketed Pad Bearing. *ASME Journal of Tribology*, 2005, **127**(4): 803–812.
- [5] P. Chen, E. Hahn. Use of Computational Fluid Dynamics in Hydrodynamic Lubrication. *Proceedings of Institute of Mechanical Engineers: Part J, Journal of Engineering Tribology*, 1998, (6): 427–435.
- [6] B. George, W. Fred. Analytical Derivation and Experimental Evaluation of Short Bearing Approximation for Full Journal Bearings. *NACA TN*, 1953, 1199–1230.
- [7] Z. Guo, H. Toshio, R. Gordon. Application of CFD Analysis for Rotating Machinery Part1: Hydrodynamic, Hydrostatic Bearings and Squeeze Film Damper. *Journal of Engineering for Gas Turbines and Power*, 2005, **127**(2): 445–451.
- [8] M. Reddi. Finite-Element Solution of the Incompressible Lubrication Problem. *ASME Journal of Lubrication Technology*, 1969, **91**(3): 524–533.
- [9] W. Sanae, H. Hirotsugu. Application of Finite Element Method to Hydrodynamic Lubrication Problems: Part 2, Finite Width Bearings. *Bulletin of the JSME*, 1971, **14**(77): 1234–1244.
- [10] W. Sanae, H. Hirotsugu, M. Masakazu. Finite Element Method to Hydrodynamic Lubrication Problems: Part 1, Infinite Width Bearings. *Bulletin of the JSME*, 1971, **14**(77): 1222–1233.
- [11] H. Toshio, Z. Guo, R. Gordon. Application of Computational Fluid Dynamics Analysis for Rotating Machinery-Part II: Labyrinth Seal Analysis. *Journal of Engineering for Gas Turbines and Power*, 2005, **127**(4): 820–826.
- [12] P. Tucker, P. Keogh. A Generalized Computational Fluid Dynamics Approach for Journal Bearing Performance Prediction. **in:** *Proceedings Institution of Mechanical Engineers: Part J, Journal of Engineering Tribology*, 3, 1994, 99–108.